



This is a repository copy of *Novel approach to forecasting photospheric emergence of active regions*.

White Rose Research Online URL for this paper:

<https://eprints.whiterose.ac.uk/199343/>

Version: Published Version

Article:

Silva, S.S.A. orcid.org/0000-0001-5414-0197, Lennard, M. orcid.org/0000-0002-1452-2577, Verth, G. orcid.org/0000-0002-9546-2368 et al. (9 more authors) (2023) Novel approach to forecasting photospheric emergence of active regions. *The Astrophysical Journal Letters*, 948 (2). L24. ISSN 2041-8205

<https://doi.org/10.3847/2041-8213/acd007>

Reuse

This article is distributed under the terms of the Creative Commons Attribution (CC BY) licence. This licence allows you to distribute, remix, tweak, and build upon the work, even commercially, as long as you credit the authors for the original work. More information and the full terms of the licence here:

<https://creativecommons.org/licenses/>

Takedown

If you consider content in White Rose Research Online to be in breach of UK law, please notify us by emailing eprints@whiterose.ac.uk including the URL of the record and the reason for the withdrawal request.



eprints@whiterose.ac.uk
<https://eprints.whiterose.ac.uk/>



Novel Approach to Forecasting Photospheric Emergence of Active Regions

S. S. A. Silva¹ , M. Lennard² , G. Verth² , I. Ballai² , E. L. Rempel^{3,4} , J. Warnecke⁵ , H. Iijima⁶ , H. Hotta⁷ ,
S.-H. Park⁸ , A. C. Donea⁹ , K. Kusano⁸ , and V. Fedun¹

¹ Plasma Dynamics Group, Department of Automatic Control and Systems Engineering, University of Sheffield, UK; suzana.silva@sheffield.ac.uk

² Plasma Dynamics Group, School of Mathematics and Statistics, University of Sheffield, Hounsfield Road, Hicks Building, Sheffield S3 7RH, UK

³ Aeronautics Institute of Technology (ITA), São José dos Campos, SP 12228-900, Brazil

⁴ National Institute for Space Research (INPE), PO Box 515, São José dos Campos, SP 12227-010, Brazil

⁵ Max-Planck-Institut für Sonnensystemforschung, Justus-von-Liebig-Weg 3, D-37077 Göttingen, Germany

⁶ Division for Integrated Studies, Institute for Space-Earth Environmental Research, Nagoya university, Furocho, Chikusa-ku, Nagoya, Aichi 464-86, Japan

⁷ Department of Physics, Graduate School of Science, Chiba university, 1-33 Yayoi-cho, Inage-ku, Chiba 263-8522, Japan

⁸ Institute for Space-Earth Environmental Research, Nagoya University, Furo-cho, Chikusa-ku, Nagoya 464-8601, Japan

⁹ School of Mathematical Sciences, Monash University, 9 Rainforest Walk, Clayton, Victoria 3800, Australia

Received 2022 November 25; revised 2023 April 21; accepted 2023 April 25; published 2023 May 15

Abstract

One key aspect of understanding the solar dynamo mechanism and the evolution of solar magnetism is to properly describe the emergence of solar active regions. In this Letter, we describe the Lagrangian photospheric flows dynamics during a simulated flux emergence that produces an active region formed by pores. We analyze the lower photospheric flow organization prior, during and following the rise of an active region, uncovering the repelling and attracting photospheric structures that act as sources and sinks for magnetic element transport. Our results show that around 10 hr before the simulated emergence, considerable global changes are taking place on mesogranular scales indicated by an increase of the number of regions acting as a source to the multiple and scattered emergences of small-scale magnetic flux. At the location of active region's appearance, the converging flows become weaker and there is an arising of a diverging region 8 hr before the emergence time. Our study also indicates that the strong concentration of magnetic field affects the flow dynamics beyond the area of the actual simulated pores, leading to complex and strongly diverging flows in the neighboring regions. Our findings suggest that the Lagrangian analysis is a powerful tool to describe the changes in the photospheric flows due to magnetic flux emergence.

Unified Astronomy Thesaurus concepts: [Solar magnetic flux emergence \(2000\)](#); [Solar active region velocity fields \(1976\)](#); [Solar convective zone \(1998\)](#)

1. Introduction

Space weather (SW) is driven, ultimately, by global solar plasma dynamics, energy generation and transport. The most significant effect of SW for humankind is via the highest-energy events, e.g., solar flares, coronal mass ejections (CMEs), high-speed solar wind and solar energetic particles. These events constitute critical hazards for space- and ground-based infrastructure: communication, navigation, research satellites, electric power networks, long-distance gas/oil pipelines, etc. (Eastwood et al. 2018). Forecasting the appearance of active regions (ARs) is essential for SW and provides a better understanding of the solar dynamo mechanisms. Research has been devoted to the study of the evolution of surface and subsurface features that aim to provide significant signatures for the emergence of intense magnetic fluxes. Helioseismic holography analysis for subsurface features shows that the local region where an AR appears is dominated by convection prior to the emergence and the emergence location would be in the intergranular region between supergranular cells and have typical flow speed smaller than actual supergranular speeds (Birch et al. 2013). Toriumi et al. (2012) estimated the horizontal velocity from Dopplergram for an AR far from the disk center and found

divergent horizontal flows 100 minutes before the emergence of the AR. Based on flow maps obtained for surface flows, granulation tracking and helioseismology, Birch et al. (2019) found that local converging horizontal flows with magnitude of about 40 m s^{-1} appear 1 day before the AR emergence. This value was obtained by averaging many AR near-surface flows prior to emergence. Due to the type of signature, i.e., converging flows, Birch et al. (2019) also concluded that there is likely an interaction between the rising flux concentrations and supergranule-scale plasma flows. Using a convolutional neural network based on line-of-sight magnetograms of regions prior to the emergence and quiet Sun magnetograms, Dhuri et al. (2020) obtained a credible model describing the evolution of the AR for up to 3 hr prior to emergence. Their model suggests that small-scale and intense fields are one of the signatures of the flux emergence.

To this day, most of the investigations on the observable signatures prior to the appearance of ARs rely on properties of subsurface flows. Some of such studies are largely based on Eulerian description and averaging properties of the subsurface and/or photospheric flows, e.g., Birch et al. (2019). This averaging process may lead to losing essential features of the complex coupling between magnetic fields and plasma flows. Also, Eulerian descriptions only take instantaneous velocity fields into consideration, describing the velocity and other dynamical variables at fixed positions and time frames. Therefore, the Eulerian approach misses some important information on the dynamics of the flow, such as barriers to



Original content from this work may be used under the terms of the [Creative Commons Attribution 4.0 licence](#). Any further distribution of this work must maintain attribution to the author(s) and the title of the work, journal citation and DOI.

transport in the flow; see, e.g., Coulliette et al. (2007). Lagrangian tools consider the temporal evolution of particles under the velocity field for a finite-time interval with length Δt . Thus, the Lagrangian analysis provides a better description of the flow's behavior in finite timescales as it considers the interaction of plasma flows and magnetic fields to identify material surfaces (3D flows) and lines (2D flows) thereby created. The most influencing material surfaces/lines are called Lagrangian coherent structures (LCSs) and they act as flow barriers, separating regions of distinct plasma dynamics. A flow can support different kinds of LCSs and these may be locally the most attracting/repelling material surfaces/lines and can also be identified as Lagrangian vortices or material lines/surfaces with minimum shear. Together, the set of different identified LCS defines the “flow skeleton.” An Eulerian analysis precludes identifying those lasting material surfaces/lines and, thereby, they do not provide a description of the “flow skeleton.” Although there are some Eulerian techniques that can be used to reveal the flow organization, those are short-term limits of LCSs for the case $\Delta t \rightarrow 0$; see, e.g., Serra & Haller (2016). Moreover, some important features described by the LCS are actually not captured at all by an Eulerian description. Studies by Coulliette et al. (2007) and Beron-Vera et al. (2013) found that Lagrangian results recovered from LCS differ dramatically from the Eulerian description of the fluid where one directly analyzes the time series of velocity fields. In an example provided by Haller (2015), if one employs Eulerian descriptors to analyze a rotating saddle using just a sequence of instantaneous velocity field snapshots, it can be wrongly identified as a vortex. Defining the underlying LCS responsible for organizing the flow is a fundamental step toward uncovering the intricate interplay between flows and magnetic fields.

The last few decades have seen an intense development of techniques for detecting LCS that uncover the hidden aspects of surface flow dynamics and provide precise information on existing photospheric transport barriers (see, e.g., Haller 2015). The application of LCS in conjunction with solar plasma flows is currently limited to a small number of studies focusing on understanding vortex dynamics and magnetic elements transport in quiet Sun regions. The 2D Lagrangian analysis of photospheric flows showed the considerable influence of the flow skeleton on the magnetic field distribution in the meso/supergranular cells (Yeates et al. 2012; Chian et al. 2014, 2019). Most recently, LCS diagnostics showed that long duration vortices appear in the gaps regions of Lagrangian chaotic saddles (Chian et al. 2020). In contrast to previous considerations of only instantaneous flows, our novel approach for the description of photospheric flows involves the determination of the flow barriers given by distinguished material lines that compose the flow's Lagrangian Skeleton.

In this study we identify the structures that shape the horizontal surface flow transport prior and during the simulated AR emergence. Since Birch et al. (2019) interpreted his findings as an interaction between the rising flux tubes and supergranular cells, we focused our analysis on identifying the most attracting and repelling LCS, as those are connected to meso- and supergranular cells' boundary and centers (Yeates et al. 2012; Chian et al. 2019). Plasma flows are intrinsically related to the evolution of fields; therefore, our analysis provides an unprecedented new approach for understanding the evolution of solar magnetism. Another promising aspect of our

analysis is that it does not require subsurface data and can be performed based only on photospheric flows. Although current velocity field data need long integration times, with the advent of high spatial-time resolution observations, the Lagrangian diagnosis will also become a possible tool to apply to actual solar flows. Our paper is organized as follows: in Section 2 we present the numerical model and the finite-time Lyapunov methodology used to identify the attracting/repelling LCS. The results of our investigation are presented in Section 3. Finally, our results are analyzed, discussed, and summarized in Section 4.

2. Methodology

2.1. R2D2 Code

The numerical data set used in our analysis were obtained by the R2D2 code (Hotta & Iijima 2020), which solves the 3D radiative magnetohydrodynamic equations. The simulated surface is placed at $z = 0$, and the vertical domain covers the range from the base of the convective zone at $z = -0.29 R_{\odot}$, to 700 km above the photosphere with varying grid spacing. The horizontal xy plane covers a $98.304 \times 98.304 \text{ Mm}^2$ area, with a resolution of 96 km. Further information on the code and the specific simulation can be found in the study by Hotta & Iijima (2020). This simulation was chosen as it was the first attempt to introduce a domain that covers the entire convective zone, allowing minimum influence of boundary conditions on the sunspot formation. The domain is periodic in the x - and y -directions and the magnetic field is set to a potential field at the top boundary.

Initially, a force-free flux tube is placed in the center of the computational domain at about 35 Mm below the photosphere. The magnetic field strength at the center of the flux tube is set to 10^4 G . The temporal evolution of intensity and the vertical magnetic field at the simulated solar surface ($z = 0.0$) Mm is shown in Figure 1. The emergence time of the AR is $t = 0 \text{ hr}$ and it is based on the definition given by Leka et al. (2013), i.e., the time at which the unsigned magnetic flux reaches 10% of the maximum magnetic flux. As indicated by Figure 1(a), the flux emergence leads first to small pores 3.3 hr before the emergence time. Then, the flux emergence is observed as solar pores with spatial scales similar to the one found in observations (Suetterlin 1998), i.e., around 2000–5000 km in size

2.2. Finite-time Lyapunov Exponents

The repelling and attracting skeleton of photospheric flows can be revealed by applying forward (f) and backward (b) finite-time Lyapunov exponents (FTLEs) to the simulated horizontal flow of the solar atmosphere obtained by R2D2. The FTLE characterizes the amount of stretching about the particles' trajectories, which is useful for tracking the evolution of the flow skeleton (i.e., flow material surfaces/lines acting as barriers, separating regions of distinct plasma dynamics), due to the emergence of magnetic flux concentrations. Advecting the fluid elements forward in time provides the forward FTLE (fFTLE), and, thereby, the repelling LCSs that are the ridges of the fFTLE. The photospheric regions that act like sinks, in the sense that they attract plasma and magnetic elements, can be found by advecting a particle backward in time. Thereby, the backward FTLE (bFTLE) reveals the attracting LCS. The ridges of the FTLE field define the material lines that delimit

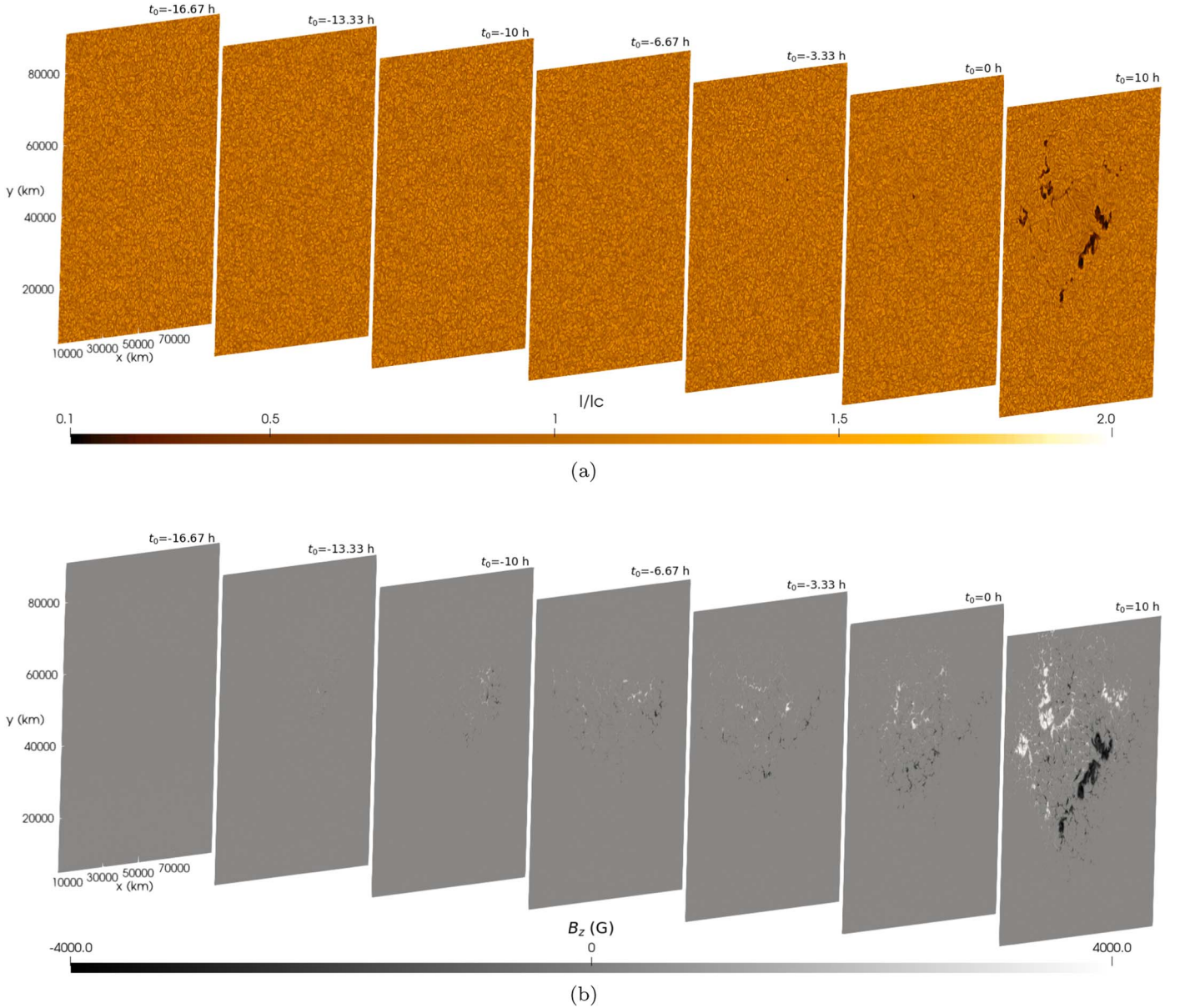


Figure 1. Evolution of the simulated solar surface, $z = 0.0$ Mm, before and after the AR emergence time, $t = 0.0$ hr, colored by: (a) continuum intensity, I , normalized by the average of the continuum intensity over the field of view, I_c ; (b) vertical component of the magnetic field, B_z .

regions under different dynamics. The positions of fluid elements are calculated by means of the advection equation

$$\frac{d\mathbf{r}}{dt} = \mathbf{v}(\mathbf{r}, t), \quad (1)$$

where \mathbf{r} is the position of the fluid patch and \mathbf{v} is the flow velocity, which in our analysis is the simulated 2D horizontal photospheric flow. Although we do not describe the 3D FTLE field, previous studies in solar physics have shown that 2D description is enough to provide important information on the flow's influence on magnetic topology and magnetic element transport (e.g., Yeates et al. 2012; Chian et al. 2014, 2019). Initially, the patches are positioned along the grid points of the simulation. Then, the fluid elements are advected from their initial position, \mathbf{r}_0 , to their final position $\mathbf{r}(t_0 + \tau)$ after a finite-time duration τ . The FTLEs of the particle trajectories are

calculated at each initial position \mathbf{r}_0 as

$$\sigma_i^{t_0+\tau}(\mathbf{r}_0) = \frac{1}{|\tau|} \ln \sqrt{|\lambda_i|}, \quad i = 1, 2, \quad (2)$$

where λ_i ($\lambda_1 > \lambda_2$) are the eigenvalues of the finite-time right Cauchy–Green deformation tensor $\Delta = J^T J$, in which $J = d\phi_{t_0}^{t_0+\tau}(\mathbf{r})/d\mathbf{r}$ is the deformation gradient, T denotes the transpose, and $\phi_{t_0}^{t_0+\tau}: \mathbf{r}(t_0) \rightarrow \mathbf{r}(t_0 + \tau)$ is the flow map for Equation (1).

3. Results

Both backward and forward FTLE fields were calculated using $\tau = 20$ minutes and $\tau = 1$ hr 40 minutes starting at $t_0 = -25$ hr. Only the x - and y -components of the velocity field at $z = 0$ are used to advect particles with Equation (1). Figure 2(a) displays the bFTLE field for a selected region of the

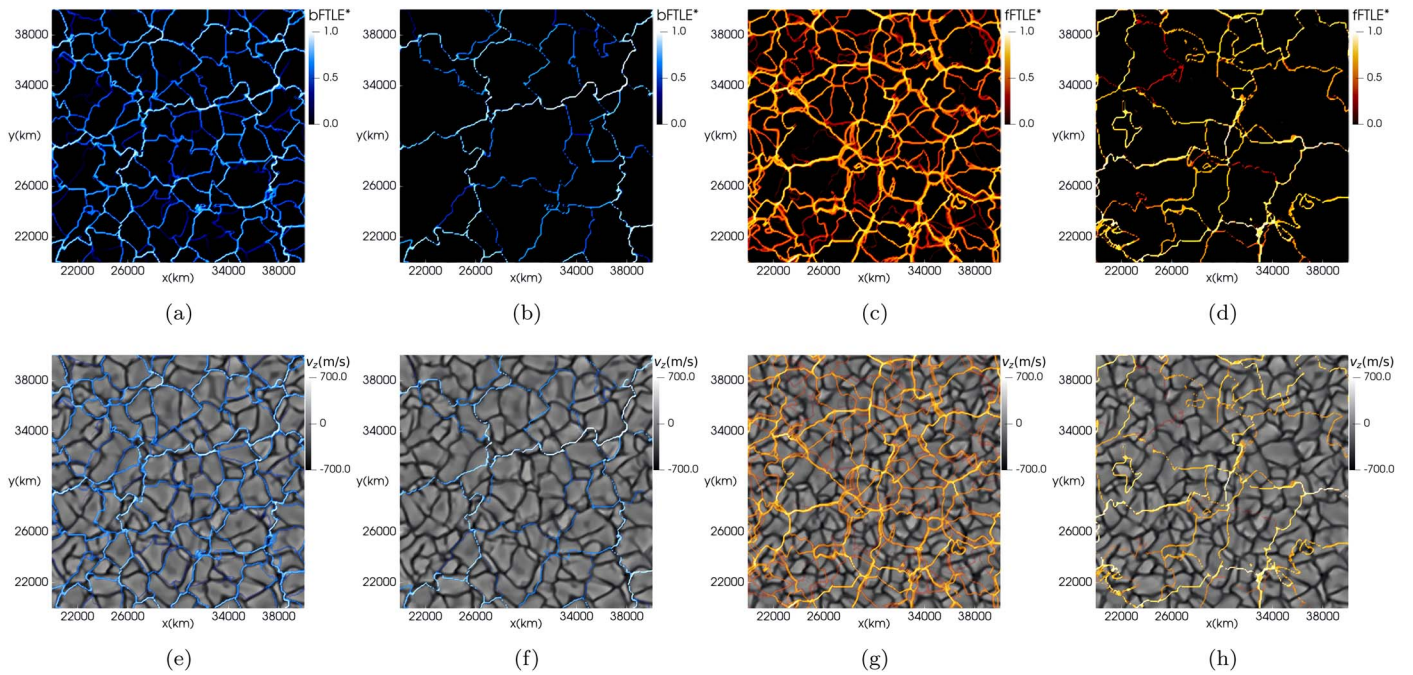


Figure 2. Selected region from the original domain colored by (a) bFTLE field starting at $t_0 = -25$ hr for $\tau = 20$ minutes; (b) Same as panel (a), but for $\tau = 1$ hr 40 minutes; (c) fFTLE field starting at $t_0 = -25$ hr for $\tau = 20$ minutes; (d) Same as panel (c), but for $\tau = 1$ hr 40 minutes; (e) ridges of the bFTLE field showed in panel (a) superimposed on the v_z at $t = t_0 = -25$ hr; (f) ridges of the bFTLE field showed in panel (b) superimposed on the v_z at $t = t_0 = -25$ hr; (g) ridges of the fFTLE field showed in panel (c) superimposed on the v_z at $t = t_0 = -25$ hr; (h) ridges of the fFTLE field showed in panel (d) superimposed on the v_z at $t = t_0 = -25$ hr.

domain calculated for $\tau = 20$ minutes, whereas the bottom panel, (e), shows the bFTLE field superimposed on the v_z at $t = t_0 = -25$ hr. Figure 2 (b) is similar to panel (a), but for $\tau = 1$ hr 40 minutes. It is clear that the ridges of the bFTLE field for an integrated time of 20 minutes reveal the Lagrangian intergranular regions. Furthermore, for $\tau = 1$ hr 40 minutes the bFTLE provides the Lagrangian boundaries of mesogranular cells. The fFTLE field is displayed in Figure 2(c) for $\tau = 20$ minutes, and in Figure 2(d) for $\tau = 1$ hr 40 minutes. Figures 2(g) and (h) show that the Lagrangian centers of nearby granular (mesogranular) cells are interconnected by ridges of the fFTLE for $\tau = 20$ minutes ($\tau = 1$ hr 40 minutes). Therefore, the ridges of fFTLE are surrounded by valleys dominated by converging flows, whereas the ridges of bFTLE are interspersed by diverging flows.

To analyze changes in photospheric flow prior to and during the simulated AR emergence, we calculated the backward and forward FTLE fields for granular and mesogranular scales, $\tau = 20$ minutes and $\tau = 1$ hr 40 minutes, respectively. We started our analysis at $t_0 = -25$ hr and calculated the FTLE field up to $t_0 = 3.67$ hr every 50 frames. As the cadence of the data is 120 s, the FTLE was calculated every 1 h and 40 minutes. In Figure 3, the blue line represents the normalized average distance of FTLE peaks (local maxima), P_d^* , as a function of t_0 and it is normalized by the mean distance of the peaks of the first 10 hr of the analysis. The time evolution of P_d^* is shown for the backward, (a) and (c), and forward, (b) and (d), FTLE field peaks (the ridges of local maxima) for $\tau = 20$ minutes and $\tau = 1$ hr 40 minutes, respectively. The maximum value of the z -component of the magnetic field at the simulated surface for the same t_0 , is represented by the orange lines. While in the granular scales the peak distances of the FTLE fields oscillate around 1.0, the mesogranular fFTLE presents closer peaks as a function of time starting at $t_0 = -10$ hr. Physically, our findings indicate that the

emergence of the magnetic flux tube is preceded by an increase in the number of regions in the surface acting as sources.

The two panels in Figures 4 and 5 show the forward and backward FTLE, respectively. The analysis were carried out for time frames in the interval $t_0 = -16.67$ hr to $t_0 = 10.0$ hr. The panels (a) in Figures 4 and 5 show the FTLE fields for $\tau = 1$ hr 40 minutes and for the panels (b) in Figures 4 and 5 the integration was computed for $\tau = 20$ minutes. The white rectangle depicts the earliest local visible feature in fFTLE that allows forecasting the AR appearance. For $\tau = 1$ hr 40 minutes, the fFTLE presents a significant signature around 8 hr prior to the emergence time and about 5 hr before the appearance of micropores at $t_0 = -3.33$ hr. For $t_0 = -10$ hr we can already see the appearance of some magnetic elements, but the average flux in the white square is less than a couple of hundred G. Therefore, the features visible in FTLE within that region can be considered as precursor for the appearance of stronger magnetic fluxes that will lead to the pore formation. For granular scales, the fFTLE presents a local distinct feature around 5 hr in advance of AR emergence. The fFTLE signature is basically a change of sign, from negative to positive values. The negative values of FTLE appear due to small eigenvalues of the Cauchy–Green deformation, i.e., the minimum FTLE values are linked to lower stretching about the trajectory of the particle in the given time interval. In other words, the minimum value of the fFTLE (bFTLE) field is connected with regions presenting converging (diverging) flows (Haller & Sapsis 2011). In regions where both forward and backward integration has a minimum, the particles’ trajectories present minor divergence from each other. Therefore, increasing the minimum of the fFTLE field means less converging flows and increased complexity for convective cells. As for the bFTLE displayed in Figure 5, the local changes are only visible after the emergence of the AR, showing strong attracting regions localized at strong magnetic field regions. Comparing Figures 1

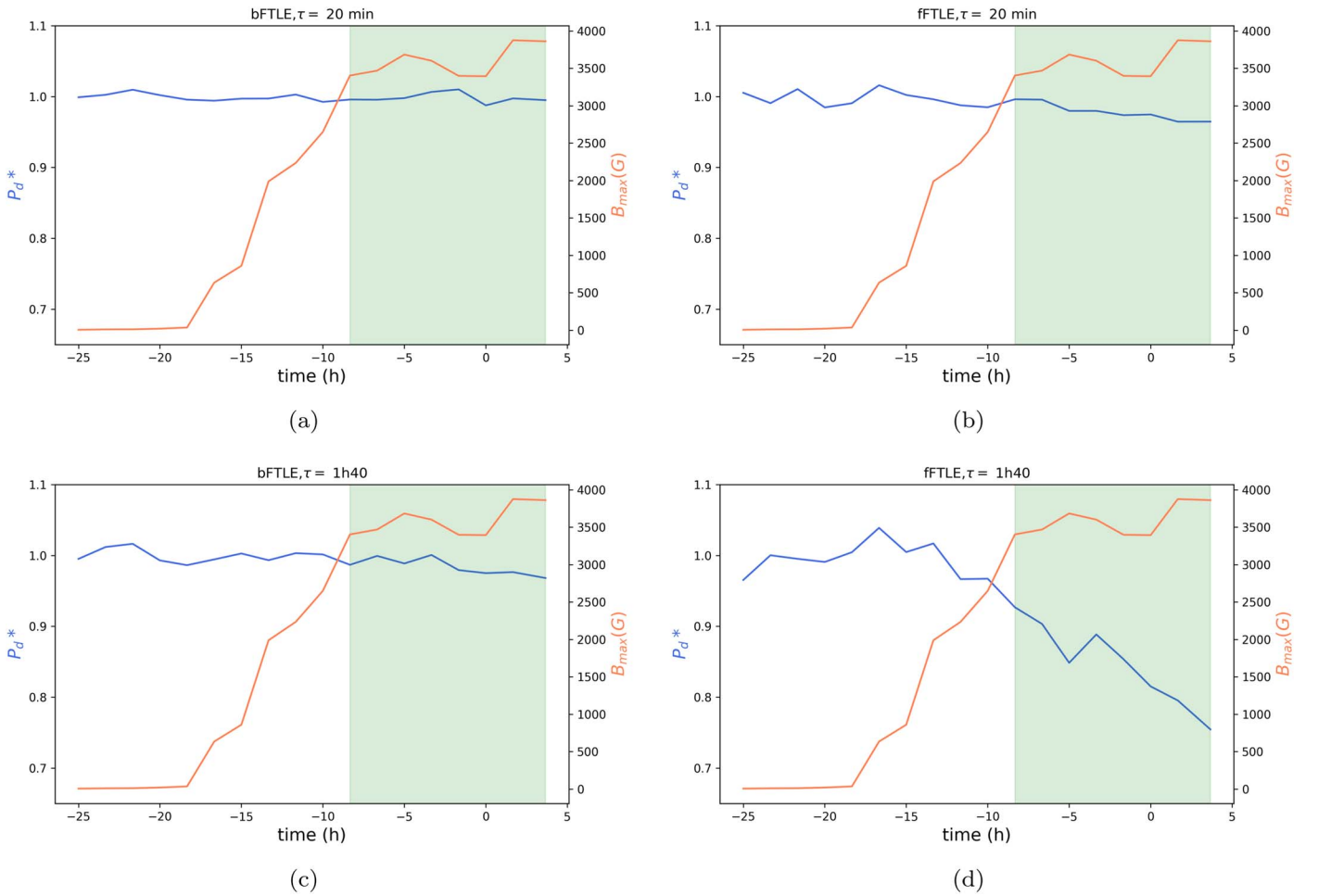


Figure 3. Normalized average distance of FTLE peaks (local maxima), P_d^* , as a function of t_0 . P_d^* is normalized by the mean distance of the peaks of the first 10 hr of the analysis. The blue line is the average peak distance of bFTLE, $\tau = 20$ minutes (a) and $\tau = 1$ hr 40 minutes (c), and fFTLE, $\tau = 20$ minutes (b) and $\tau = 1$ hr 40 minutes (d) starting at different t_0 shown in x -axis. The orange line is the maximum value of the z -component of the magnetic field at the simulated surface at each t_0 . The green region indicates the times t_0 where $B_{\max} \geq 3500$ G.

and 4, it is clear that at mesogranular scales the strong concentration of magnetic field influences the repelling flows surrounding the high magnetic flux regions. Figure 5 indicates that the effect of the strong concentration of magnetic flux on attracting regions is only local (just in the case of pores) or between the pore regions. The presence of strong repelling regions around the pores is in line with observational studies that show that the opposite polarities of an AR tend to diverge from each other during the emergence phase up until the total flux reaches its maximum, e.g., Wang & Sheeley (1989), Kosovichev & Stenflo (2008), and van Driel-Gesztelyi & Green (2015).

4. Discussion and Conclusions

Our study addresses, for the first time, the problem of photospheric flows prior to and during a simulated AR emergence using a Lagrangian analysis. The simulation assumes a flux tube rising to the surface from the convection zone via buoyancy. Our findings have deep implications for the current understanding of the influence of the rising magnetic flux tubes on the convection processes. Results indicate considerable global disturbances in the dynamics of the mesogranular cells due to the intense magnetic flux rising below the surface. Those changes are marked by the substantial

variance of the distance of fFTLE peaks at mesogranular scales, which is detectable around 10 hr prior to the emergence of the magnetic field. The time evolution of the fFTLE field indicates that the simulated flows are becoming less converging in different parts of cells and that their dynamic has increased complexity, as FTLE becomes positive in large regions of the flow field. The change in plasma flows captured by fFTLE may be due to the fact that the initially uniformly weak horizontal fields develop into a mixture of weak magnetic fields (Lites et al. 1998), which naturally would increase the complexity of flow dynamics and lead to fFTLE becoming positive in regions where it was previously negative.

The FTLE detects local changes in the mesogranular cells dynamics as distinct features in the fFTLE field, around 8 hr before the emergence time at the location of AR appearance. The local changes of FTLE indicate a region dominated by converging flows getting weaker and the appearance of repelling regions. Those local signatures are also visible for granular cells around 5 hr before the flux emergence. The appearance of positive fFTLE in the neighborhood of the emergence location implies that cells tend to drive apart as the rising flux approaches the solar surface. At the same time, there is no visible disturbance in the attracting lines of the bFTLE, which delimits the boundary of cells and thereby indicates the intergranular region. This corroborates the scenario of an

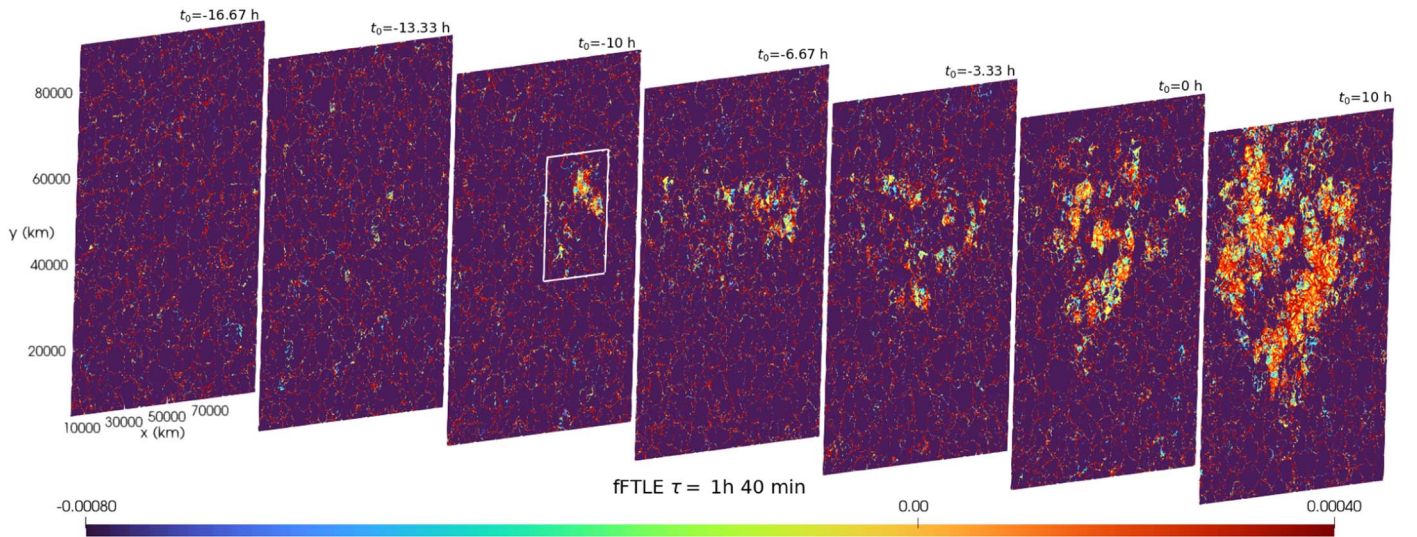
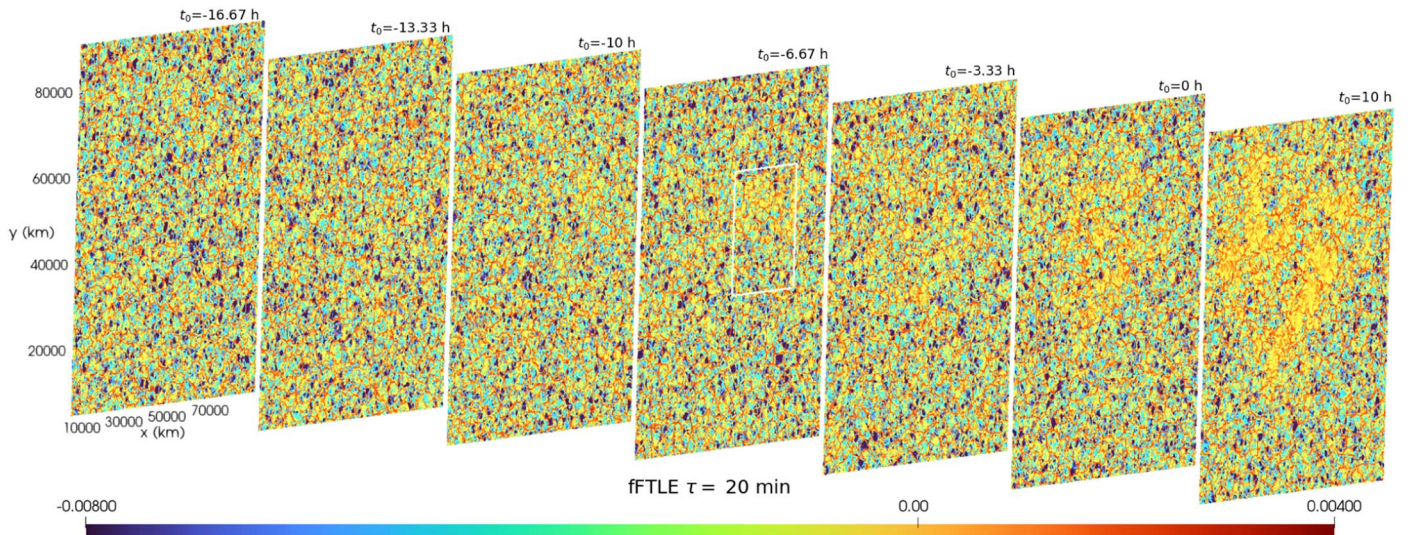
(a) fFTLE with $\tau = 1 \text{ h } 40 \text{ min}$ (b) fFTLE with $\tau = 20 \text{ min}$

Figure 4. Evolution of the simulated solar surface, $z = 0.0 \text{ Mm}$, before and after the AR emergence time, $t = 0.0 \text{ hr}$, colored by the fFTLE field. The time t_0 indicates the initial time used for the calculation of fFTLE. The white rectangle indicates the location and time of the first local signature prior to the AR emergence.

emerging flux tube in the intergranular lanes as suggested by Birch et al. (2013). It is worth mentioning that for the same data set, Hotta & Iijima (2020) did not find any local changes in the divergence flow before the AR formation.

Our findings suggest that, while still below the photosphere, the rising magnetic flux tube can impact the dynamics of convective cells at the surface as the number of source regions in the flow increases. This expands to smaller scales, granular and mesogranular, the analysis carried out by Birch et al. (2019), where they found a local interaction between the emerging magnetic field and supergranular motion. Their convergence flow region covered an area of 40 Mm by 20 Mm , whereas we found a local signature region with half of the size, with dimensions around 20 Mm by 10 Mm . The global signature, i.e., the decrease between fFTLE peaks, was observed for mesogranular flows with size around 5 times greater than typical granular scales. The fFTLE field also indicates that the intense magnetic field concentration affects a

region much greater than the actual pores, leading to diverging flows in broad regions surrounding the strong magnetic flux tubes. On the other hand, the magnetic concentration only creates strong attracting regions where the magnetic fluxes are present in the intergranular lanes.

One of the advantages of applying FTLE to describe flow changes prior to AR formation is that it does not need information on subsurface flows or averaging a velocity field obtained from observational data over a long time. Furthermore, as the changes observed by FTLE do not only appear at the emergence site, forecasting becomes more accessible as the global signatures are present in regions covering the entire simulation domain, 90 Mm by 90 Mm . Although the leading time of 8 hr is shorter than 1 day found by supergranular-scale horizontal flow (e.g., Birch et al. 2019), the fFTLE, as a measure of the complexity in small-scale horizontal flow, may still be a unique tool to investigate the possible relation between small-scale flow and large-scale flux emergence.

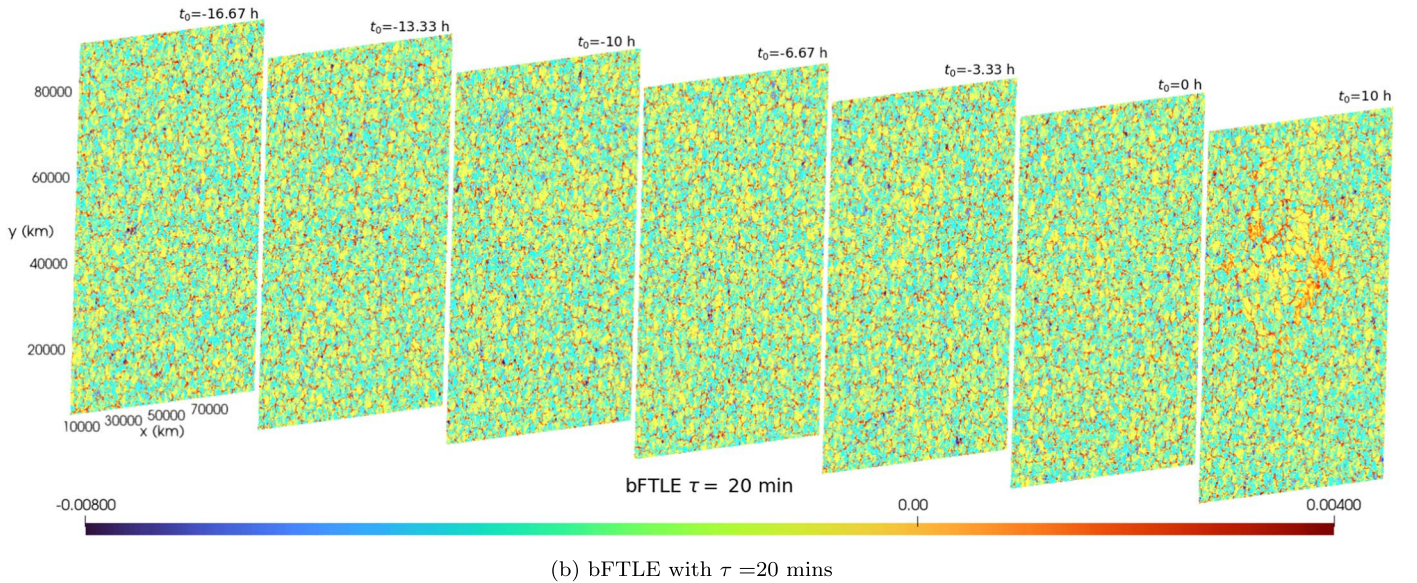
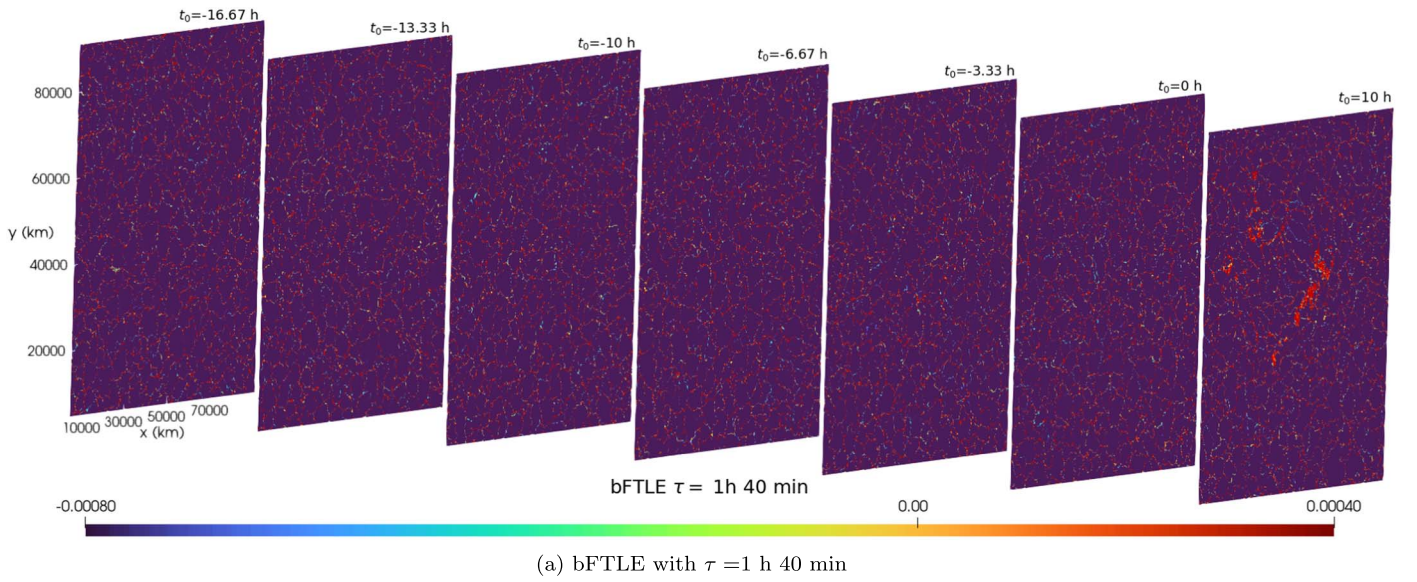


Figure 5. The same as in Figure 4, but here we show corresponding bFTLE.

However, one current difficulty in performing Lagrangian diagnosis based on solar observation data is the long integration time (around 7 hr) required to establish the material lines organizing the flow (Chian et al. 2014, 2019) when applying local correlation tracking techniques (November & Simon 1988; Fisher & Welsch 2008; Giagkiozis et al. 2018) to recover the velocity field. Future works should focus on higher spatial-time resolution velocity field reconstruction that allows a better description of the flow dynamics by LCS. Finally, our results strongly underline that the FTLE is a powerful tool to describe the changes in the photospheric flow dynamics due to magnetic flux emergence, and we believe this technique should be widely applied in order to provide a valuable statistical database, as already suggested by Roudier et al. (2021). Analogous to traditional hydrology, which is the study of the movement and distribution of water on Earth, the techniques used in this paper potentially open up a new field of magnetohydrology of the solar atmosphere.

V.F., G.V., I.B., E.R., and S.S.A.S. are grateful to The Royal Society, International Exchanges Scheme, collaboration with Brazil (IES\R1\191114). V.F., G.V., and S.S.A.S. are grateful to Science and Technology Facilities Council (STFC) grant ST/V000977/1. V.F. and G.V. thank The Royal Society, International Exchanges Scheme, collaboration with Chile (IE170301) for support provided. V.F., G.V., I.B., and A.C.D. acknowledge the support by The Royal Society, International Exchanges Scheme, collaboration with Australia (IES/R3/213012). E.L.R. acknowledges Brazilian agencies CAPES and CNPq (grants 88887.309065/2018-01 and 306920/2020-4, respectively) for their financial support. M.L. is grateful to STFC for the PhD studentship project reference (2489787). This research has also received financial support from the ISEE, International Joint Research Program (Nagoya University, Japan) and European Union's Horizon 2020 research and innovation program under grant agreement No. 824135 (SOLARNET). For this work J.W. has received funding from the European Research Council (ERC)

under the European Union’s Horizon 2020 research and innovation program (grant agreement No. 818665 “UniSDyn”). V.F. and H.I. are grateful to S. Shelyag for help with data transfer.

ORCID iDs

S. S. A. Silva  <https://orcid.org/0000-0001-5414-0197>
 M. Lennard  <https://orcid.org/0000-0002-1452-2577>
 G. Verth  <https://orcid.org/0000-0002-9546-2368>
 I. Ballai  <https://orcid.org/0000-0002-3066-7653>
 E. L. Rempel  <https://orcid.org/0000-0002-4971-5854>
 J. Warnecke  <https://orcid.org/0000-0002-9292-4600>
 H. Iijima  <https://orcid.org/0000-0002-1007-181X>
 H. Hotta  <https://orcid.org/0000-0002-6312-7944>
 S.-H. Park  <https://orcid.org/0000-0001-9149-6547>
 A. C. Donea  <https://orcid.org/0000-0002-4111-3496>
 K. Kusano  <https://orcid.org/0000-0002-6814-6810>
 V. Fedun  <https://orcid.org/0000-0002-0893-7346>

References

- Beron-Vera, F. J., Wang, Y., Olascoaga, M. J., Goni, G. J., & Haller, G. 2013, *JPO*, **43**, 1426
- Birch, A. C., Braun, D. C., Leka, K. D., Barnes, G., & Javornik, B. 2013, *ApJ*, **762**, 131
- Birch, A. C., Schunker, H., Braun, D. C., & Gizon, L. 2019, *A&A*, **628**, A37
- Chian, A. C.-L., Rempel, E. L., Aulanier, G., et al. 2014, *ApJ*, **786**, 51
- Chian, A. C.-L., Silva, S. S. A., Rempel, E. L., et al. 2019, *MNRAS*, **488**, 3076
- Chian, A. C. L., Silva, S. S. A., Rempel, E. L., et al. 2020, *PhRvE*, **102**, 060201
- Coulliette, C., Lekien, F., Paduan, J. D., Haller, G., & Marsden, J. E. 2007, *EnST*, **41**, 6562
- Dhuri, D. B., Hanasoge, S. M., Birch, A. C., & Schunker, H. 2020, *ApJ*, **903**, 27
- Eastwood, J. P., Hapgood, M. A., Biffis, E., et al. 2018, *SpWea*, **16**, 2052
- Fisher, G. H., & Welsch, B. T. 2008, in ASP Conf. Ser. 383, Subsurface and Atmospheric Influences on Solar Activity, ed. R. Howe et al. (San Francisco, CA: ASP), 373
- Giagkiozis, I., Fedun, V., Scullion, E., Jess, D. B., & Verth, G. 2018, *ApJ*, **869**, 169
- Haller, G. 2015, *AnRFM*, **47**, 137
- Haller, G., & Sapsis, T. 2011, *Chaos*, **21**, 023115
- Hotta, H., & Iijima, H. 2020, *MNRAS*, **494**, 2523
- Kosovichev, A. G., & Stenflo, J. O. 2008, *ApJL*, **688**, L115
- Leka, K. D., Barnes, G., Birch, A. C., et al. 2013, *ApJ*, **762**, 130
- Lites, B. W., Skumanich, A., & Martinez Pillet, V. 1998, *A&A*, **333**, 1053
- November, L. J., & Simon, G. W. 1988, *ApJ*, **333**, 427
- Roudier, T., Švanda, M., Malherbe, J. M., et al. 2021, *A&A*, **647**, A178
- Serra, M., & Haller, G. 2016, *Chaos*, **26**, 053110
- Suetterlin, P. 1998, *A&A*, **333**, 305
- Toriumi, S., Hayashi, K., & Yokoyama, T. 2012, *ApJ*, **751**, 154
- van Driel-Gesztelyi, L., & Green, L. M. 2015, *LRSP*, **12**, 1
- Wang, Y. M., & Sheeley, N. R. 1989, *SoPh*, **124**, 81
- Yeates, A. R., Hornig, G., & Welsch, B. T. 2012, *A&A*, **539**, A1